

## 49. GEOCHEMISTRY AND PETROLOGY OF IGNEOUS ROCKS, DEEP SEA DRILLING PROJECT LEG 62<sup>1</sup>

K. E. Seifert, Department of Earth Sciences, Iowa State University, Ames, Iowa  
T. L. Vallier, U.S. Geological Survey, Menlo Park, California  
K. E. Windom, Department of Earth Sciences, Iowa State University, Ames, Iowa  
and  
S. R. Morgan,<sup>2</sup> U.S. Geological Survey, Menlo Park, California

### ABSTRACT

Igneous rocks were recovered from three sites on Hess Rise during Deep Sea Drilling Project Leg 62: altered basalt at Site 464, at the northern end of Hess Rise; and altered trachyte from Site 465, and rounded basalt pebbles in upper Albian to middle Miocene sediments from Site 466, both at the southern end of Hess Rise. Major-, minor-, and trace-element data for basalt from Hole 464 are consistent with these rocks being transitional tholeiites that have undergone low-temperature alteration by reaction with sea water. Trachyte from Hole 465A exhibits as many as three generations of plagioclase along with potash feldspar that are flow aligned in groundmasses altered to smectites and random mixed-layer clays. Textural evidence indicates that these rocks were erupted subaerially. Chemical data show a range of values when plotted on two- and three-component variation diagrams. The observed variations may result in part from differentiation, but they also reflect the high degree of alteration. Several oxides and elements show strong correlation with  $H_2O^+$ :  $K_2O$ ,  $SiO_2$ , Rb and Lu decrease and MgO increases with increasing  $H_2O^+$ . These trends, except for that of Lu, are consistent with experimentally determined changes in chemistry that accompany alteration. The trend for Lu has not been previously reported; it may result from a more-intense alteration of the HREE-rich mafic minerals than of the LREE-rich feldspars. Despite their alteration, the trachytes compare favorably with alkalic differentiates from oceanic islands.

We interpret Hess Rise as a volcanic platform formed by eruption of off-ridge volcanic rocks onto MORB oceanic crust during the Aptian and Albian stages, after the basement had migrated away from the spreading center. By analogy with present oceanic islands, we propose that early tholeiitic basalts were followed by alkalic basalts and their differentiation products (trachytes), producing a volcanic archipelago of islands and seamounts. Subsequent tectonism and subsidence led to the present state of Hess Rise.

### INTRODUCTION

Igneous rocks were recovered at Sites 464, 465, and 466, although only as clasts from sediments at Site 466. Site 464 (39°52'N, 173°53'E) is near the north end of the northwest-southeast-trending part of Hess Rise, whereas Sites 465 (33°49'N, 178°55'E) and 466 (34°11'N, 179°15'E) are near the southern end of Hess Rise, near the junction between the northwest-southeast ridge and the ridge which trends east-northeast to west-southwest (Fig. 1). Hess Rise is bounded on the west by the Emperor Seamounts and on the northeast by the Emperor Trough, which is parallel to the northwest-southwest ridge. The Mendocino Fracture Zone truncates Hess Rise on the south. The lack of a clear magnetic anomaly sequence on Hess Rise is best explained by the fact that it lies within the Cretaceous magnetic quiet zone; this suggests that it is younger than early Aptian (about 111 m.y.). Our drilling results and plate reconstructions (Lancelot and Larson, 1975; Lancelot, 1978) indicate that Hess Rise formed in pre-late-Albian time south of the equator.

Hess Rise is one of several regions in the central and north-central Pacific Ocean that do not fit the normal age-depth curve (Sclater et al., 1971). This suggests that Hess Rise consists in part of volcanic products from later intraplate volcanism that are superimposed on normal oceanic crust; thus, the igneous rocks collected probably represent the upper layers of the later volcanism and not normal mid-ocean ridge basalt (MORB). Site 464 has provided samples of the northwest-southeast trending ridge, and Sites 465 and 466 samples of the ridge which trends east-northeast and west-southwest. The petrology and chemistry of these samples can be used to help interpret the origin of Hess Rise.

At Site 466, rounded basalt pebbles were recovered in cores 10, 11, 12, 14, 17, 20, 27, 28 and 29 of middle Eocene to late Albian cherty nannofossil ooze and chalk. The basalt is vesicular, the vesicles ranging from almost spherical to ovoid. The fresher basalts are gray, but more-altered basalts exhibit a yellow color. Microprobe analyses of pyroxenes indicate the basaltic pebbles are alkalic and transitional, rather than tholeiitic. A more-detailed description of these pebbles is given by Vallier et al. (this volume).

### STUDY TECHNIQUES

The petrography of igneous rocks recovered from Holes 464 and 465A was studied in thin section and by X-ray diffraction. The

<sup>1</sup> Initial Reports of the Deep Sea Drilling Project, Volume 62.

<sup>2</sup> Current address: Department of Geology, Western Washington University, Bellingham, Wa. 98225.

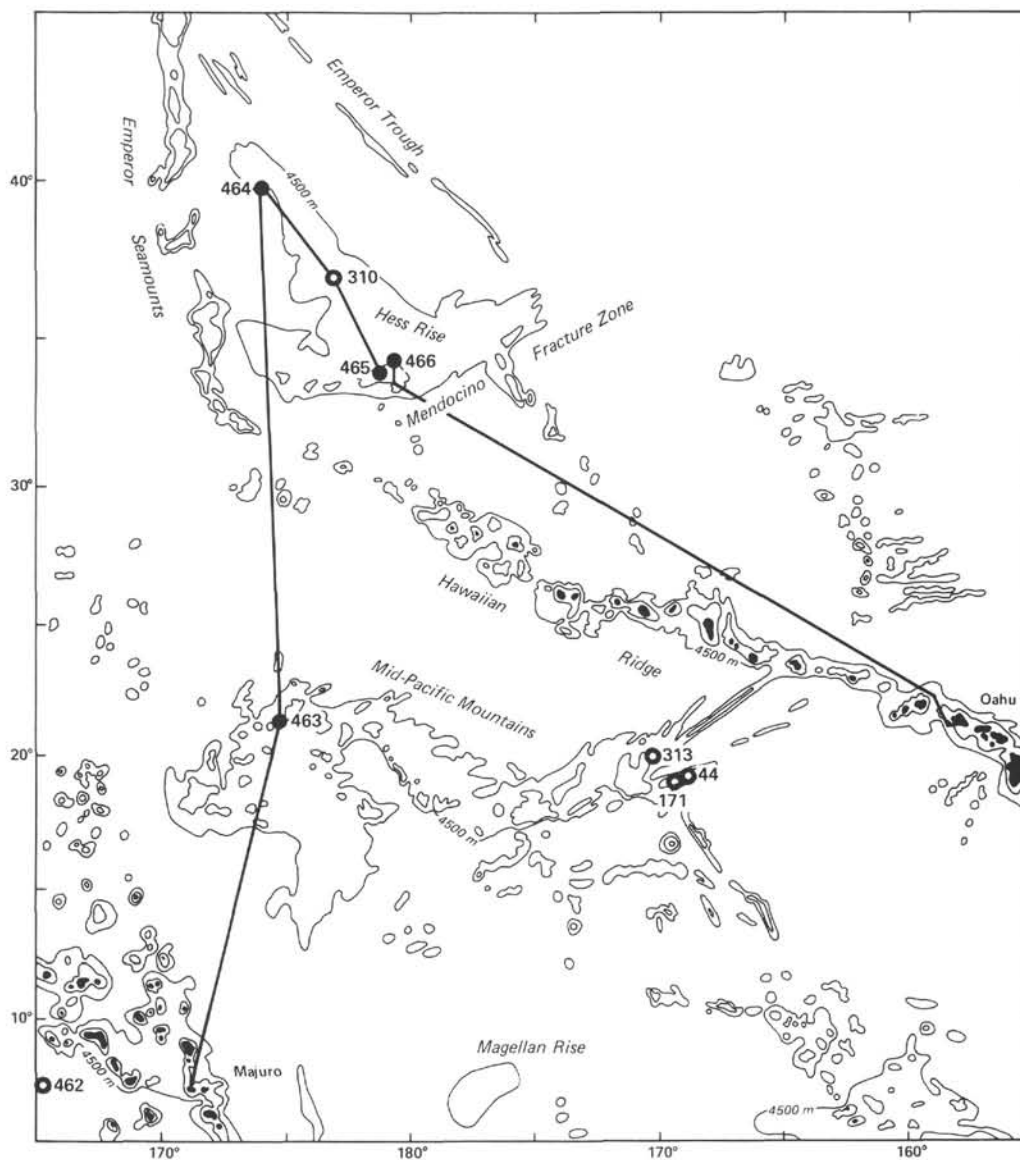


Figure 1. Chart of the region covered by DSDP Leg 62, showing the location of drilled sites.

geochemistry was determined by a combination of X-ray fluorescence (XRF) and instrumental neutron-activation analysis (INAA) techniques. The major- and minor-element oxides  $\text{SiO}_2$ ,  $\text{Al}_2\text{O}_3$ ,  $\text{FeO}$  (total iron as  $\text{FeO}$ ),  $\text{MgO}$ ,  $\text{CaO}$ ,  $\text{Na}_2\text{O}$ ,  $\text{K}_2\text{O}$ ,  $\text{TiO}_2$ , and  $\text{MnO}$ ; and trace elements Zr, Cr, Ni, Ba, and Sr were determined by X-ray fluorescence. The major-element oxides  $\text{FeO}$  and  $\text{Na}_2\text{O}$  and the trace elements La, Ce, Sm, Eu, Tb, Yb, Lu, Cr, Sc, Co, Rb, Ba, Th, Hf, Ta, and Sr were determined by instrumental neutron-activation analysis. The reported  $\text{Na}_2\text{O}$  values are those obtained from INAA, and the Cr, Ba, and Sr values are averages of values obtained from the two techniques. XRF and INAA analyses for Hole 465A samples are from splits of the same powder. Hole 464 analyses are from the same samples, but separate powders.

The method of X-ray spectroscopy used by the USGS laboratory at Menlo Park is described below, and the estimated relative errors and detection limits for several oxides are given in Table 1.

Each sample is dried to remove adsorbed moisture, then ground to  $-100$  mesh. A 1-gram sample of the powdered rock is weighed into a platinum-gold crucible along with 6 grams of lithium tetraborate flux and  $1\frac{1}{2}$  grams of anhydrous lithium nitrate. The three ingredients are stirred with a teflon stir bar until a visually homogeneous mixture has been achieved. Four drops of 10% bromic acid are added to the mixture as an anti-wetting agent.

The crucibles are covered and fused at  $500^\circ\text{C}$  for 4 min, and at  $1050^\circ\text{C}$  for 28 min. Fused discs are removed from the crucibles after cooling, then weighed. The weight is compared with the known volatile content of the flux to determine the loss on fusion (LOF) value of the rock.

The discs are polished on an automatic grinding unit for 15 min, using boron carbide as the abrasive. Polished discs are cleaned in an ultrasonic tank filled with distilled water for 2 to 3 min, rinsed in distilled water, and washed with ethol alcohol to remove grit from the polishing stage and any grease from handling. Polished discs are analyzed in the Diano 8600 unit for major oxides, and in the Diano 710 unit for minor oxides. Working curves using 19 rock standards are used for each element. Major-element determinations are corrected for absorption and enhancement, and minor-element determinations are corrected for absorption, enhancement, spectral line, interference, and background, according to standard USGS analytical procedure.

The method of instrumental neutron-activation analysis (INAA) is very similar to that described by Jacobs et al. (1977). Powdered samples are irradiated simultaneously with USGS standards (BCR-1, BHVO-1, and GSP-1) and an internal standard (OB-1). Samples and standards are irradiated in pure synthetic quartz (Suprasil) tubes. Following irradiation, the samples and standards are counted twice, first at 5 to 10 days to obtain La, Sm, Yb, Lu, Na, U, and Ba; and

Table 1. Relative error and detection limits for 10 major and five trace oxides at the X-Ray Spectroscopy Laboratories, USGS, Menlo Park, California.

| Oxide                          | Relative Error (%) | Detection Limit (ppm oxide) |
|--------------------------------|--------------------|-----------------------------|
| SiO <sub>2</sub>               | 0.36               | 125                         |
| Al <sub>2</sub> O <sub>3</sub> | 0.98               | 200                         |
| Fe <sub>2</sub> O <sub>3</sub> | 0.74               | 27                          |
| MgO                            | 2.39               | 205                         |
| CaO                            | 1.09               | 28                          |
| Na <sub>2</sub> O              | 1.68               | 700                         |
| K <sub>2</sub> O               | 1.58               | 10                          |
| TiO <sub>2</sub>               | 1.74               | 23                          |
| P <sub>2</sub> O <sub>5</sub>  | 4.55               | 50                          |
| MnO                            | 2.41               | 10                          |
| NiO                            | 5.8                | 10                          |
| Cr <sub>2</sub> O <sub>3</sub> | 5.0                | 15                          |
| BaO                            | 6.3                | 10                          |
| ZrO                            | 4.2                | 20                          |
| SrO                            | 2.8                | 20                          |

Note: Reports of five trace oxides are rounded off as follows:

| Oxide                          | Report of Nearest | At Greater Than |
|--------------------------------|-------------------|-----------------|
| NiO                            | 5 ppm             | 10 ppm          |
| Cr <sub>2</sub> O <sub>3</sub> | 10 ppm            | 20 ppm          |
| BaO                            | 10 ppm            | 10 ppm          |
| ZrO                            | 10 ppm            | 20 ppm          |
| SrO                            | 10 ppm            | 20 ppm          |

again at 30 to 40 days to obtain Ce, Eu, Tb, Rb, Sr, Cs, Fe, Co, Sc, Th, Cr, Hf, and Ta. The precision is estimated to be better than  $\pm 5\%$  for all elements except Tb, Yb, Lu, Ta, Th, and Hf, which are estimated to be within  $\pm 15\%$ .

Total H<sub>2</sub>O, H<sub>2</sub>O<sup>-</sup>, CO<sub>2</sub>, and FeO were obtained by a variety of techniques. Total H<sub>2</sub>O was measured using the Penfield method, in which the sample is fused with PbO, PbCrO<sub>4</sub>, and CuO at 1000°C, and the last water is driven off with an oxygen torch. H<sub>2</sub>O<sup>-</sup> is obtained by measuring weight loss when the sample is heated to 105 to 110°C in a platinum crucible. H<sub>2</sub>O<sup>+</sup> is determined by subtracting H<sub>2</sub>O<sup>-</sup> from total H<sub>2</sub>O. CO<sub>2</sub> is determined with a Leco Wr-12 analyzer. Ferrous iron is analyzed by fusion of the sample with HF and H<sub>2</sub>SO<sub>4</sub>. Boric acid and phosphoric acid are added to complex the fluoride and stop oxidation, and the solution is titrated with 0.1N potassium dichromate.

X-ray diffraction studies of Hole 465A samples were conducted on aliquots of the same powder used for XRF and INAA study. The powder was mixed with distilled water, and the slurry was subjected to an ultrasonic probe for 10 min. This ensured that individual particles were thoroughly dispersed. The resulting suspension was placed in a settling column with additional distilled water and allowed to settle. After a minimum of 7 hours, the top 10 cm was decanted, and the particular matter was plated onto a porous ceramic tile, using a vacuum system. X-ray-diffraction patterns were taken from the coated tile—first from the untreated samples and later, after the samples were saturated with ethylene glycol.

## SITE 464

### Introduction

Sixteen cm of basalt was recovered below lower Albian limestone in Hole 464 before drilling was terminated because of a stuck drill string. The recovered basalt fragments are extensively altered, and many of the primary minerals have been replaced. The depth

from which basalt fragments were recovered coincides with the top of a strong acoustic reflector. Air-gun seismic-reflection profiles suggest that acoustic layering continues below this boundary, perhaps indicating some interlayering of sedimentary and igneous rocks. Geochemistry was determined from three samples, and four plagioclase crystals were microprobed (Lee-Wong, this volume) from a piece from 464-34, CC, 21 cm. The plagioclase ranges approximately from An<sub>46</sub> to An<sub>54</sub>.

### Data

The geochemistry of Hole 464 basalts is given in Table 2. Only INAA results were obtained for Sample 2, and the FeO value listed is actually FeO<sub>t</sub>. The analyzed basalts are tholeiitic, but highly altered. The H<sub>2</sub>O<sup>+</sup> values of 2.79 and 2.74% are much higher than the values of 0.1 to 0.2% for fresh tholeiites (Hart, 1971). Also, the Fe<sub>2</sub>O<sub>3</sub>/(FeO + Fe<sub>2</sub>O<sub>3</sub>) ratios of 0.91 and 0.97 are much higher than the ratio 0.3, regarded as typical of fresh tholeiites (Engel et al., 1965; Shido et al., 1971). These data and the abundance of smectites strongly suggest a high degree of alteration by ocean water at low temperatures (Bass, 1976; Andrews, 1977; Scheidegger and Stakes, 1977). The abundance of K<sub>2</sub>O (1.68 and 0.81%), compared to about 0.22% for fresh tholeiites (Cann, 1971), is also best explained by low-temperature alteration. CaO and SiO<sub>2</sub> have values far below those regarded as typical of fresh tholeiites; CaO is very low. However, MgO values are close to those expected of fresh tholeiite. Studies on the alteration of tholeiitic basalt by sea water (Hart, 1970; Andrews, 1977; Scarfe and Smith, 1977) have shown that the basalt experiences an increase in H<sub>2</sub>O<sup>+</sup>, total Fe, K, and Ti, and a decrease in Ca, Mg, and SiO<sub>2</sub>. Seyfried and Bischoff (1979) obtained similar results in experiments at 70°C, except that the basalt in their experiments *gained* Mg slightly. The major- and minor-element chemistry for Site 464 basalts is thus consistent with their being altered tholeiites.

The most-convincing evidence that these basalts are tholeiitic rather than alkalic is the REE pattern (Figure 2). This REE pattern is relatively flat at X15 chondrite abundance and corresponds to a transitional MORB (Sun et al., 1979). In contrast, alkalic basalts show considerable LREE enrichment relative to HREE. Low-temperature alteration also increases LREE relative to HREE (Frey et al., 1973; Ludden and Thompson, 1978). However, from our data, we cannot tell if the tholeiite is a MORB or an oceanic-island tholeiite that was erupted onto pre-existing oceanic crust.

## SITE 465

### Introduction

Approximately 24 meters of trachyte was recovered from acoustic basement below upper Albian limestone in Hole 465A. The trachyte is highly vesicular, with vesicles up to 5 mm in diameter. Red iron-oxide staining is present, and there is a lack of glassy flow margins in recovered samples. These features suggest a subaerial origin. The trachytes are highly brecciated in the upper-

Table 2. Major-, minor-, and trace-element geochemistry of DSDP Leg 62 Hess Rise igneous rocks.

| Sample Hole Section Interval or piece (cm) | 1<br>464<br>34,CC<br>13-14 | 2<br>464<br>34,CC<br>19-21 | 3<br>464<br>34,CC<br>23-25 | 4<br>465A<br>41-3<br>P9 | 5<br>465A<br>42-1<br>123-125 | 6<br>465A<br>42-2<br>90-93 | 7<br>465A<br>42-3<br>84-86 | 8<br>465A<br>43-1<br>64-66 | 9<br>465A<br>43-1<br>91-95 | 10<br>465A<br>43-1<br>114-117 | 11<br>465A<br>43-1<br>144-148 | 12<br>465A<br>43-2<br>65-68 | 13<br>465A<br>44-1<br>78-81 | 14<br>465A<br>44-2<br>P5 | 15<br>465A<br>44-3<br>121-124 | 16<br>465A<br>45-1<br>99-102 | 17<br>465A<br>45-2<br>113-116 | 18<br>465A<br>45-3<br>P11 | 19<br>465A<br>45-4<br>P13A | 20<br>465A<br>46-1<br>36-39 | 21<br>465A<br>46-2<br>5-8 | 22<br>465A<br>46-3<br>P2 |
|--|----------------------------|----------------------------|----------------------------|-------------------------|------------------------------|----------------------------|----------------------------|----------------------------|----------------------------|-------------------------------|-------------------------------|-----------------------------|-----------------------------|--------------------------|-------------------------------|------------------------------|-------------------------------|---------------------------|----------------------------|-----------------------------|---------------------------|--------------------------|
| SiO <sub>2</sub> (wt. %)                   | 46.75                      | —                          | 45.58                      | 58.07                   | 59.77                        | 59.79                      | 59.96                      | 59.23                      | 58.67                      | 59.06                         | 59.22                         | 60.81                       | 60.29                       | 59.79                    | 59.5                          | 60.34                        | 60.39                         | 59.68                     | 58.99                      | 60.25                       | 56.54                     | 60.07                    |
| TiO <sub>2</sub>                           | 1.75                       | —                          | 1.72                       | 1.02                    | 0.99                         | 0.99                       | 1.02                       | 1.03                       | 1.06                       | 1.05                          | 1.05                          | 1.02                        | 1.02                        | 1.07                     | 1.0                           | 1.03                         | 1.01                          | 1.03                      | 1.02                       | 1.07                        | 0.95                      | 1.06                     |
| Al <sub>2</sub> O <sub>3</sub>             | 15.69                      | —                          | 16.14                      | 18.68                   | 18.47                        | 18.87                      | 18.81                      | 18.73                      | 18.60                      | 18.80                         | 18.71                         | 18.80                       | 18.64                       | 18.92                    | 18.4                          | 19.08                        | 18.74                         | 18.88                     | 19.03                      | 18.89                       | 17.76                     | 19.02                    |
| Fe <sub>2</sub> O <sub>3</sub>             | 6.49                       | —                          | 6.27                       | 2.60                    | 2.22                         | 2.70                       | 2.29                       | 2.12                       | 2.36                       | 2.22                          | 2.70                          | 1.98                        | 1.89                        | 2.11                     | 1.83                          | 1.87                         | 2.01                          | 2.23                      | 2.16                       | 1.97                        | 1.70                      | 2.24                     |
| FeO  | 7.16                       | 12.5 <sup>a</sup>          | 6.46                       | 0.73                    | 0.45                         | 0.28                       | 0.48                       | 0.31                       | 0.37                       | 0.46                          | 0.14                          | 0.26                        | 0.62                        | 0.62                     | 1.00                          | 0.89                         | 0.83                          | 0.94                      | 0.55                       | 0.55                        | 1.12                      | 0.71                     |
| MnO  | 0.29                       | —                          | 0.25                       | 0.02                    | 0.02                         | 0.02                       | 0.02                       | 0.02                       | 0.02                       | 0.02                          | 0.02                          | 0.02                        | 0.04                        | 0.04                     | 0.06                          | 0.04                         | 0.05                          | 0.05                      | 0.02                       | 0.04                        | 0.10                      | 0.05                     |
| MgO  | 7.89                       | —                          | 7.82                       | 2.08                    | 1.19                         | 0.87                       | 1.70                       | 1.38                       | 1.72                       | 1.48                          | 1.58                          | 0.31                        | 0.42                        | 1.24                     | 0.4                           | 0.36                         | 0.43                          | 0.79                      | 1.37                       | 0.65                        | 0.48                      | 0.53                     |
| CaO  | 3.91                       | —                          | 4.72                       | 2.33                    | 2.04                         | 2.06                       | 2.20                       | 2.32                       | 2.34                       | 2.37                          | 2.29                          | 1.94                        | 2.25                        | 2.42                     | 3.4                           | 2.30                         | 2.31                          | 2.26                      | 2.22                       | 2.28                        | 4.81                      | 2.31                     |
| Na <sub>2</sub> O                          | 3.08                       | 3.36                       | 3.38                       | 4.75                    | 5.01                         | 5.20                       | 4.87                       | 5.25                       | 4.94                       | 5.10                          | 4.98                          | 5.32                        | 5.19                        | 5.29                     | 4.68                          | 5.19                         | 5.02                          | 5.41                      | 5.12                       | 5.45                        | 4.63                      | 5.46                     |
| K <sub>2</sub> O                           | 1.68                       | —                          | 0.81                       | 2.89                    | 4.82                         | 5.06                       | 3.84                       | 4.29                       | 3.68                       | 3.92                          | 3.84                          | 6.27                        | 5.85                        | 4.20                     | 6.4                           | 5.90                         | 6.12                          | 4.93                      | 3.97                       | 5.09                        | 6.44                      | 5.15                     |
| P <sub>2</sub> O <sub>5</sub>              | 0.09                       | —                          | 0.09                       | 0.28                    | 0.33                         | 0.32                       | 0.30                       | 0.41                       | 0.31                       | 0.34                          | 0.31                          | 0.35                        | 0.36                        | 0.35                     | 0.4                           | 0.36                         | 0.35                          | 0.34                      | 0.29                       | 0.44                        | 0.46                      | 0.46                     |
| H <sub>2</sub> O <sup>+</sup>              | 2.79                       | —                          | 2.74                       | 2.51                    | 1.38                         | 1.14                       | 2.09                       | 1.42                       | 1.76                       | 1.68                          | 2.58                          | 0.86                        | 1.16                        | 2.45                     | 0.86                          | 0.84                         | 0.60                          | 1.85                      | 2.68                       | 0.92                        | 0.85                      | 1.30                     |
| H <sub>2</sub> O <sup>-</sup>              | 4.33                       | —                          | 5.31                       | 3.98                    | 2.54                         | 1.57                       | 2.95                       | 2.80                       | 3.71                       | 2.79                          | 2.03                          | 0.64                        | 0.78                        | 1.48                     | 1.02                          | 0.79                         | 1.03                          | 0.96                      | 1.47                       | 1.62                        | 0.63                      | 0.92                     |
| CO <sub>2</sub>                            | —                          | —                          | —                          | 0.37                    | 0.49                         | 0.92                       | 0.38                       | 0.36                       | 0.34                       | 0.32                          | 0.57                          | 0.59                        | 0.39                        | 0.35                     | 1.73                          | 0.60                         | 0.60                          | 0.56                      | 0.43                       | 0.21                        | 3.02                      | 0.25                     |
| Total                                      | 101.90                     | —                          | 101.29                     | 100.31                  | 99.72                        | 99.79                      | 100.91                     | 99.67                      | 99.88                      | 99.61                         | 100.02                        | 99.17                       | 98.90                       | 100.33                   | 100.7                         | 99.59                        | 99.49                         | 99.91                     | 99.32                      | 99.43                       | 99.49                     | 99.53                    |
| La (ppm)                                   | 5.08                       | 5.06                       | 4.83                       | 81.2                    | 80.3                         | 79.8                       | 83.2                       | 85.9                       | 82.6                       | 75.1                          | 80.2                          | 89.1                        | 87.3                        | 80.8                     | 83.5                          | 79.7                         | 84.4                          | 84.7                      | 76.6                       | 83.8                        | 81.8                      | 85.0                     |
| Ce   | 13.6                       | 13.2                       | 12.8                       | 156                     | 164                          | 165                        | 179                        | 173                        | 164                        | 160                           | 171                           | 167                         | 184                         | 169                      | 180                           | 164                          | 170                           | 171                       | 166                        | 183                         | 164                       | 187                      |
| Sm   | 3.08                       | 3.48                       | 3.09                       | 8.93                    | 10.6                         | 10.5                       | 9.84                       | 11.5                       | 10.5                       | 10.1                          | 10.6                          | 9.32                        | 11.5                        | 10.2                     | 11.7                          | 10.6                         | 11.4                          | 11.4                      | 9.88                       | 11.0                        | 10.6                      | 11.1                     |
| Eu   | 1.17                       | 1.19                       | 1.25                       | 2.98                    | 2.92                         | 3.01                       | 2.90                       | 3.18                       | 2.90                       | 3.11                          | 3.01                          | 2.98                        | 3.02                        | 3.13                     | 2.99                          | 2.95                         | 3.01                          | 3.05                      | 2.97                       | 3.13                        | 2.80                      | 3.13                     |
| Tb   | 0.66                       | 0.69                       | 0.68                       | 0.98                    | 1.35                         | 1.37                       | 1.10                       | 1.24                       | 1.03                       | 1.21                          | 1.08                          | 1.50                        | 1.55                        | 1.40                     | 1.35                          | 1.36                         | 1.63                          | 1.43                      | 1.24                       | 1.40                        | 1.31                      | 1.40                     |
| Yb   | 2.96                       | 2.47                       | 2.37                       | 2.02                    | 3.33                         | 3.18                       | 1.90                       | 2.80                       | 1.82                       | 2.21                          | 2.00                          | 2.24                        | 4.21                        | 2.83                     | 3.78                          | 3.59                         | 4.40                          | 3.14                      | 2.69                       | 3.53                        | 3.55                      | 3.18                     |
| Lu   | 0.42                       | 0.32                       | 0.34                       | 0.32                    | 0.53                         | 0.49                       | 0.31                       | 0.37                       | 0.30                       | 0.34                          | 0.31                          | 0.35                        | 0.64                        | 0.42                     | 0.60                          | 0.59                         | 0.69                          | 0.49                      | 0.41                       | 0.55                        | 0.59                      | 0.51                     |
| Sc   | 55.0                       | 55.8                       | 55.0                       | 2.59                    | 2.72                         | 2.82                       | 2.17                       | 2.50                       | 2.11                       | 2.32                          | 2.22                          | 2.85                        | 3.20                        | 2.32                     | 3.07                          | 2.87                         | 3.12                          | 2.86                      | 2.58                       | 3.10                        | 2.95                      | 3.16                     |
| Co   | 38.6                       | 50.3                       | 47.3                       | 8.50                    | 11.4                         | 19.6                       | 11.5                       | 10.9                       | —                          | 19.2                          | 21.5                          | 19.3                        | —                           | 19.5                     | —                             | 11.7                         | 22.6                          | 16.7                      | 12.2                       | 22.1                        | —                         | 16.1                     |
| Th   | 0.33                       | 0.23                       | 0.25                       | 10.8                    | 10.4                         | 10.9                       | 10.7                       | 10.7                       | 10.6                       | 10.9                          | 10.7                          | 10.2                        | 10.7                        | 10.7                     | 10.5                          | 10.4                         | 10.3                          | 10.5                      | 11.0                       | 10.7                        | 9.61                      | 10.5                     |
| Hf   | 3.17                       | 3.16                       | 3.16                       | 17.0                    | 16.8                         | 16.6                       | 18.9                       | 16.2                       | 18.4                       | 16.3                          | 18.5                          | 15.0                        | 16.9                        | 13.9                     | 18.1                          | 17.1                         | 17.0                          | 16.2                      | 18.3                       | 16.2                        | 15.9                      | 17.3                     |
| Ta   | 0.28                       | 0.28                       | 0.26                       | 8.42                    | 8.74                         | 8.86                       | 9.89                       | 9.22                       | 9.06                       | 8.81                          | 10.2                          | 9.38                        | 11.1                        | 8.98                     | 10.7                          | 8.81                         | 9.63                          | 9.34                      | 10.1                       | 10.9                        | 8.14                      | 10.4                     |
| Zr   | 111                        | —                          | 111                        | 681                     | 718                          | 748                        | 688                        | 770                        | 651                        | 711                           | 526                           | 474                         | 822                         | 651                      | 829                           | 770                          | 800                           | 740                       | 740                        | 770                         | 755                       | 792                      |
| Rb   | —                          | —                          | —                          | 15.3                    | 23.5                         | 28.3                       | 20.2                       | 30.8                       | 20.0                       | 20.3                          | 23.7                          | 34.3                        | 45.6                        | 23.7                     | 66.5                          | 58.9                         | 55.3                          | 33.8                      | 25.4                       | 34.3                        | 67.8                      | 45.7                     |
| Ba   | —                          | —                          | —                          | 655                     | 605                          | 596                        | 613                        | 632                        | 680                        | 688                           | 672                           | 656                         | 646                         | 673                      | 617                           | 616                          | 611                           | 680                       | 673                        | 648                         | 384                       | 652                      |
| Sr   | 158                        | 166                        | 178                        | 372                     | 276                          | 252                        | 397                        | 272                        | 349                        | 336                           | 334                           | 256                         | 318                         | 343                      | 251                           | 268                          | 285                           | 310                       | 328                        | 315                         | 215                       | 335                      |

<sup>a</sup> Total iron as FeO.

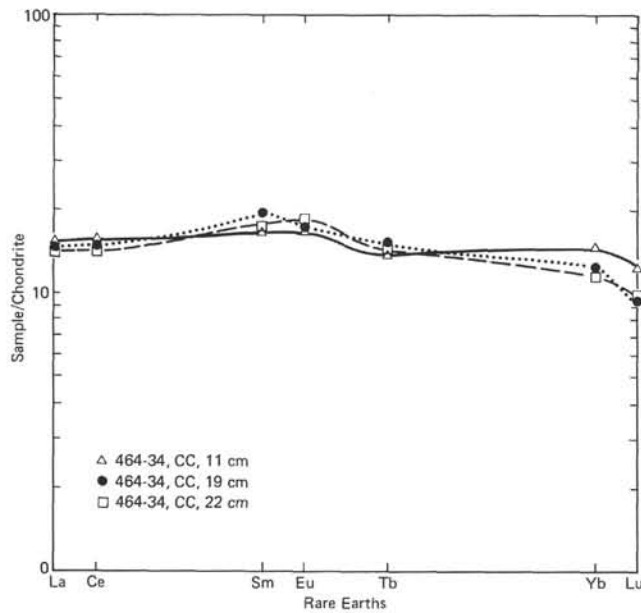


Figure 2. Normalized plot of abundance of rare-earth elements in Hole 464 basalts.

most cores and are variably altered to smectites throughout. In addition to the mineralogical changes, the geochemistry shows certain systematic changes that are best explained by alteration. The geochemistry was determined for 19 samples (Table 2) to provide data on a total of 30 elements and oxides. Microprobe analyses of 13 plagioclase crystals (Lee-Wong, this volume) from five samples of trachyte indicate a compositional range from about An<sub>28</sub> to An<sub>43</sub>.

The only primary minerals identified in the trachytes are two or three generations of plagioclase, potash feldspar, and opaque minerals (Figure 3). The feldspar laths frequently show a flow alignment. Occasionally, outlines of what may have been pyroxene crystals are observed. The groundmass in the trachyte samples is greatly altered.

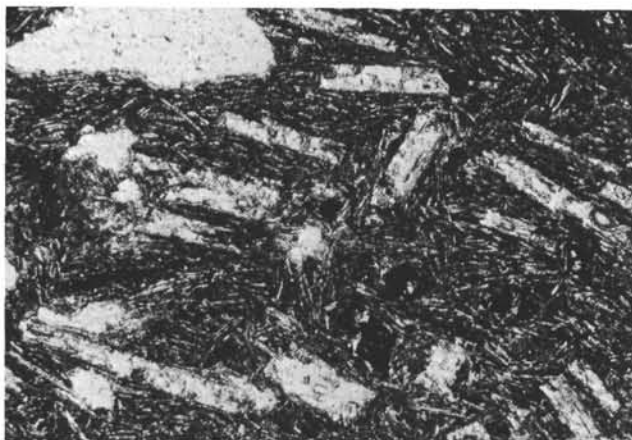


Figure 3. Photomicrograph of Hole 465A trachyte.

Data

The major-, minor-, and trace-element abundances of Hole 465A trachytes are listed in Table 2 and plotted against depth in Figure 4. Available powder from Sample 15 was insufficient to allow XRF analysis with the usual accuracy; thus, some oxide abundances for that sample are rounded to tenths of a percent. The high CaO and CO<sub>2</sub> values for Samples 15 and 19 indicate considerable calcite contamination of these samples; this is confirmed petrographically. The contamination is so great for Sample 19 that the other major oxides are drastically reduced, and this sample has not been plotted in any of the figures. Sample 15 is not as heavily contaminated with calcite and has been plotted on the figures, although it generally does not fit relationships as well as other samples. The calcite is present both in thin veins and as small disseminated crystals in some samples, making it difficult to separate completely.

SiO<sub>2</sub>, K<sub>2</sub>O, and Rb generally exhibit a slight overall increase with depth in Hole 465A, and MgO decreases (Figure 4). Al<sub>2</sub>O<sub>3</sub> and TiO<sub>2</sub> both show smaller increases with depth. No consistent variation is shown by FeO, CaO, Na<sub>2</sub>O, La, or La/Sm. Although all these data show some variation, the variation of Rb with depth is considerably greater than for any other element or oxide. Sample 43-2, 65-68 cm exhibits very high Rb and K<sub>2</sub>O values and a very low MgO content.

Plots of selected oxides and elements are given in Figure 5. In Figure 5A, MgO is observed to decrease as K<sub>2</sub>O increases, and in Figure 5B, SiO<sub>2</sub> increases as K<sub>2</sub>O increases. These trends can be explained either by dif-

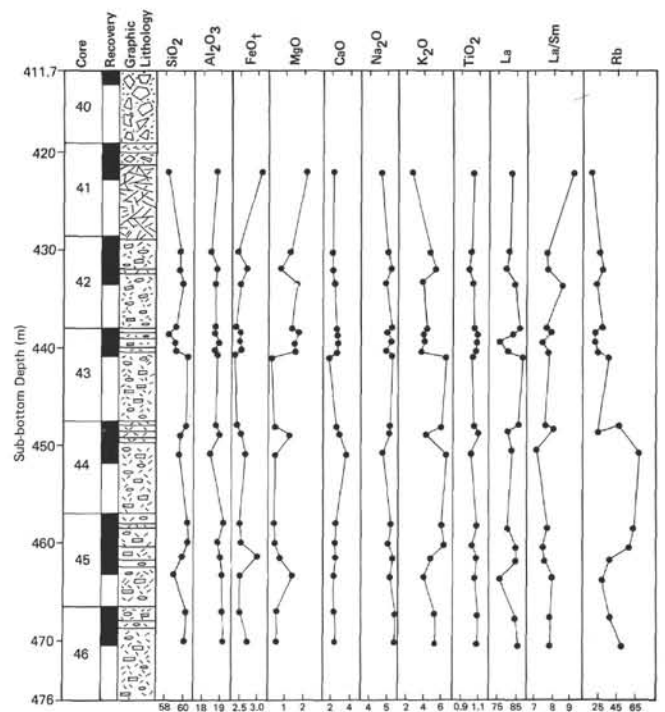


Figure 4. Variation of selected chemical data with depth in Hole 465A. Oxides are given in weight percent, and elements in ppm.

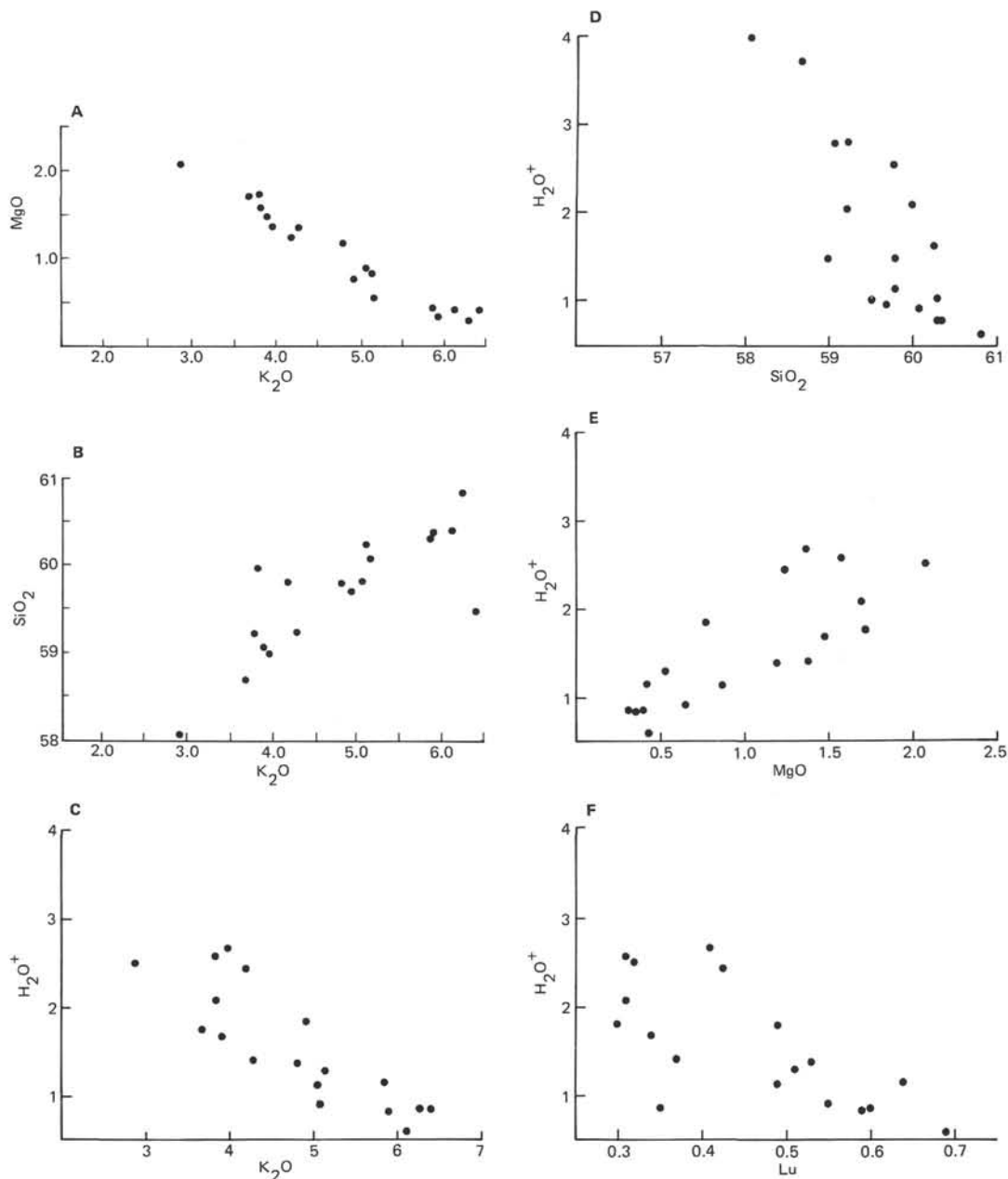


Figure 5. Plots of chemical data showing related trends. Oxides are given in weight percent, and elements in ppm.

ferentiation or high-temperature alteration. Figures 5C to 5E show that both  $K_2O$  (Fig. 5C) and  $SiO_2$  (Fig. 5D) decrease as  $H_2O^+$  increases, whereas  $MgO$  (Fig. 5E) increases as  $H_2O^+$  increases. These relationships are best explained by high-temperature ( $>150^\circ C$ ) alteration (Humphries and Thompson, 1978; Mottl and Holland, 1978). Like K, Rb decreases as  $H_2O^+$  increases. Surprisingly, Lu also decreases as  $H_2O^+$  increases (Fig. 5F), although the relationship is not as clear as those noted above. If Lu varies with  $H_2O^+$ , then so should the other HREE. The LREE do not vary systematically with  $H_2O^+$ . No good relationship was observed between  $H_2O^+$  and  $Fe_2O_3/(FeO + Fe_2O_3)$ ,  $TiO_2$ ,  $Na_2O$ ,  $CaO$ , or  $Al_2O_3$ . In summary, with increasing  $H_2O$ ,  $MgO$  in-

creases and  $K_2O$ ,  $SiO_2$ , and the HREE apparently decrease.

The extreme differentiation of these trachytes is well illustrated by Figure 6, the AFM diagram. The spread of points, however, may be more indicative of high-temperature alteration than of differentiation, although the difference is not obvious from this type of plot.

Figure 7 shows the range of REE values for the 19 analyzed samples of trachyte. The greater spread of the HREE relative to the LREE likely was caused by high-temperature alteration (as suggested by Fig. 5F), although such an effect has never been reported before, to the authors' knowledge. The HREE mobility exhibited in these trachytes is probably best explained by

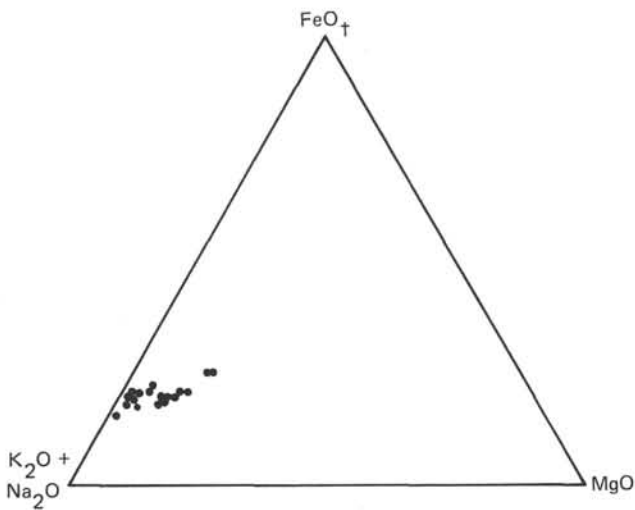


Figure 6. Plot of Hole 465A trachytes on an AFM diagram.

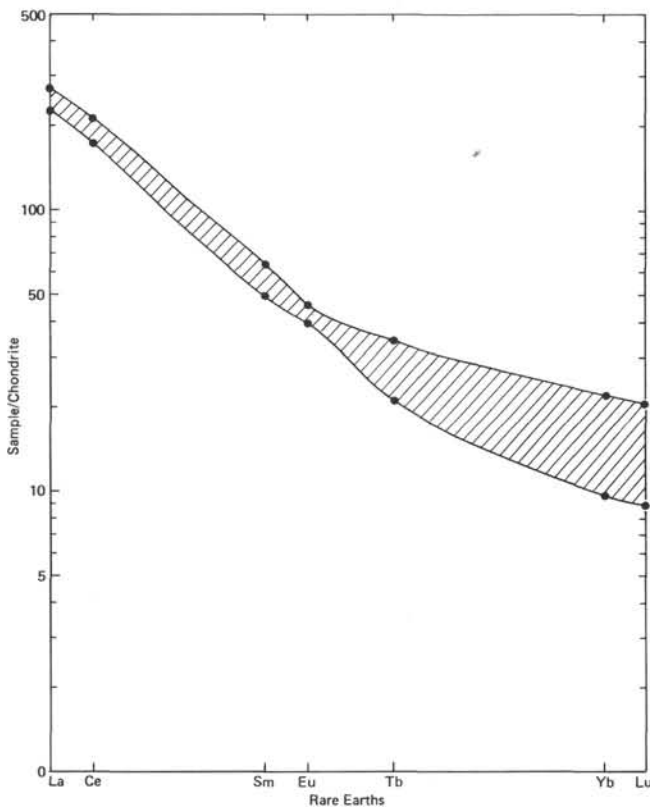


Figure 7. Normalized plot of the total range of rare-earth-element abundance in Hole 465A trachytes. The greater spread of HREE relative to LREE appears to be due to high-temperature alteration.

the extreme alteration of the HREE-rich mafic minerals (Fig. 3), whereas the LREE-rich feldspars are much less altered.

Eight samples were studied to determine the nature of the alteration material. All studied samples have a highly altered groundmass and yielded X-ray diffraction patterns interpreted as mixtures of smectite and

random-mixed-layer (RML) clays. Diffraction peaks are broad, ranging from about 10 to 30 Å. Although sharp, definitive peaks were not obtained, the most reproducible discerned peaks occur at 15, 17, 18.4, and 22 Å.

Treatment of the 8 samples with ethylene glycol yielded a variety of results. In general, the glycolated samples did not yield peaks below about 14 Å, and in about half of the samples the large composite peak was tightened up slightly. Both untreated and glycolated samples gave patterns with major peaks around 17 and 22 Å.

The X-ray-diffraction results are best explained by a mixture of smectite and RML clays. The ubiquity of 20-to 30-Å peaks indicates a large component of RML clays, and the reduction of peaks less than about 17 Å in glycolated samples indicates smectite. To our knowledge, the alteration of trachyte in the marine environment has not been studied; however, both smectite and RML clays are common products of low-temperature alteration of basalt (Bass, 1976; Scarfe and Smith, 1977; Seyfried et al., 1976, 1978). However, their presence does not preclude higher-temperature alteration. Montmorillonite was found as an alteration product formed by the reaction of basalt and seawater at 200°C and 500 bars (Bischoff and Dickson, 1975). Thus, the clay minerals may have formed during the hypothesized high-temperature alteration, which is suggested by the major- and minor-element data, or they may have formed by weathering subsequent to initial cooling.

## Discussion

Despite their alteration, the Hole 465A trachytes are similar to trachytes found on many other oceanic islands. In Figure 8, the Hess Rise rocks are compared to a suite of differentiated alkaline volcanic rocks from the Tristan da Cunha group (Baker, 1973). The Tristan da Cunha trend is classified as moderately alkaline by Baker. If only the least-altered trachytes (lowest  $H_2O^+$ ) from Hess Rise are considered in each figure, an excellent fit to the Tristan da Cunha group plots is obtained. This is not evidence that the fit is significant, because the lowest  $H_2O^+$  value (0.60%) still may represent extensive alteration. Nevertheless, the fit is excellent on several plots. Note that the least-altered Hess Rise samples (upper right) fall directly on Tristan da Cunha group samples on an  $SiO_2$ -MgO plot (Fig. 8A). In Figure 8B, the least-altered samples are on the extreme right and again fall on the Tristan da Cunha group plot. Similar results are obtained for plots of  $FeO_1$ -MgO (Fig. 8C) and CaO-MgO (Fig. 8D). In Figure 8E ( $K_2O$ -MgO), the least-altered samples again fall directly on the Tristan da Cunha group plot, even though our results suggest that  $K_2O$  and MgO are the oxides most drastically affected during alteration. Figure 8F is the only plot in which the Hess Rise samples do not directly overlap the Tristan da Cunha group samples, and it appears that the  $Na_2O$  values for the Hess Rise rocks are too low. This may be due to a small, consistent reduction of  $Na_2O$  by alteration in the Hess

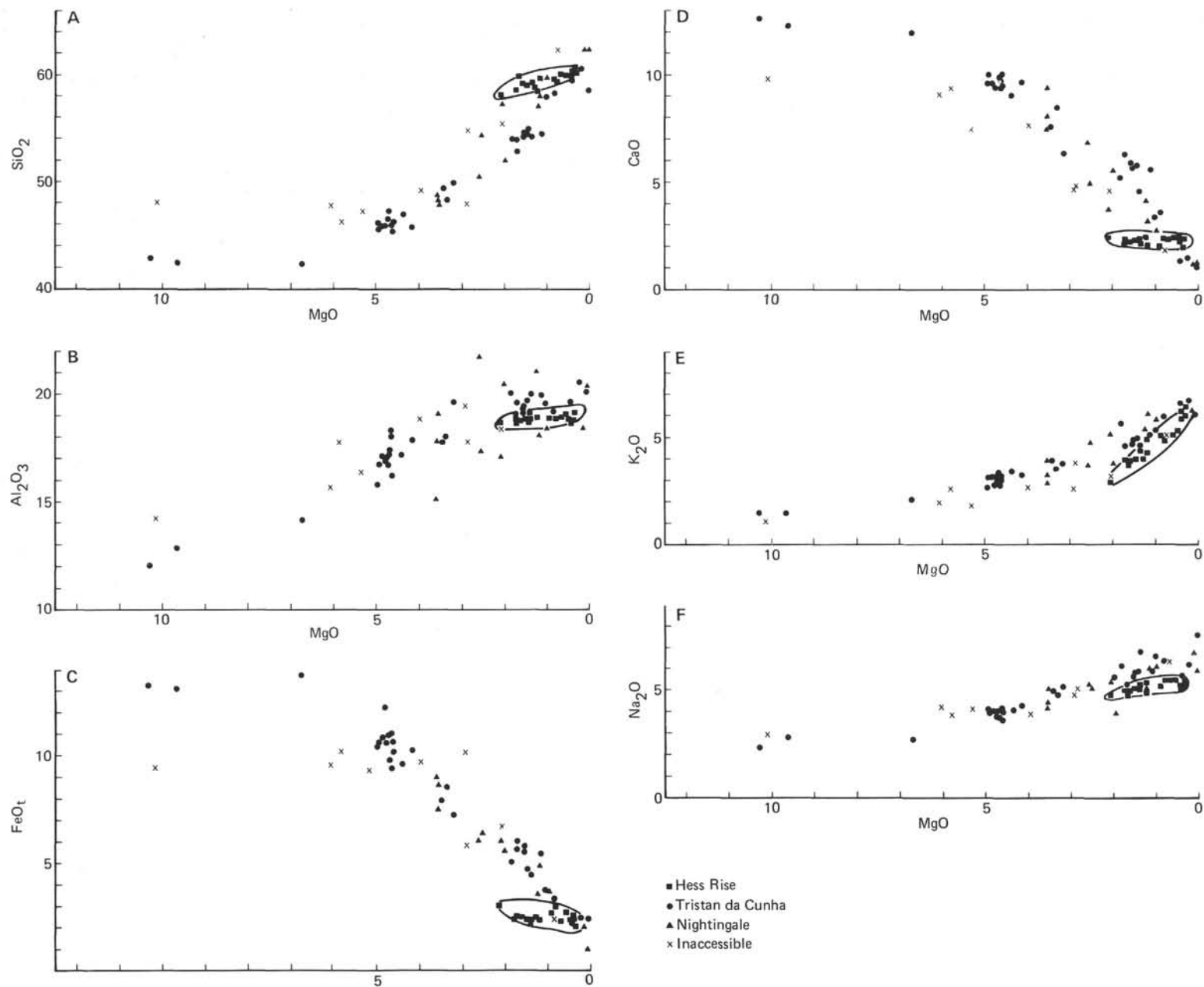


Figure 8. Chemical parameters of Hole 465A trachytes compared to those of alkaline rocks of the Tristan de Cunha group (Baker, 1973). Oxides are given in weight percent.

Rise samples, or they may have had a slightly lower primary Na<sub>2</sub>O content. Despite the Na<sub>2</sub>O deficiency, the chemistries of the Hess Rise rocks and the more-differentiated rocks of the Tristan da Cunha group are very close.

### CONCLUSIONS

Tholeiitic and alkalic basalts and trachytes were recovered from Hess Rise during DSDP Leg 62. Such a variety of volcanic rocks on Hess Rise indicates off-ridge volcanism superimposed on normal MORB basement. The trachyte is the result of alkalic differentiation. Intermediate differentiates between trachyte and alkali basalt that could provide evidence of the trend of differentiation (Miyashiro, 1978) were not recovered.

Correlative variations of SiO<sub>2</sub>, K<sub>2</sub>O, MgO, and Lu as a function of H<sub>2</sub>O<sup>+</sup> for trachytes recovered from Hole 465A indicate that these rocks have been altered. The decrease of SiO<sub>2</sub> and K<sub>2</sub>O and the increase of MgO with increasing H<sub>2</sub>O<sup>+</sup> is in agreement with chemical trends found in experimental studies of high-temperature alteration. The apparent decrease of Lu with increasing H<sub>2</sub>O<sup>+</sup> has not been reported previously and appears to indicate mobility of HREE during the high-temperature alteration of these trachytes. The abundant smectite and RML clays are compatible with either high- or low-temperature alteration.

Subaerial eruption of the trachyte flows at Site 465 is suggested by vesicles greater than 5 mm in diameter, red iron-oxide staining, and the absence of glassy flow margins. Thus, Hess Rise is a subsided volcanic archipelago and probably consists of both drowned oceanic islands and seamounts. The volcanic archipelago most likely formed during the Aptian and Albian ages. The similarity of ages of the oldest sedimentary rocks at the northern (Site 464) and southern (Site 465) ends of Hess Rise precludes a hot-spot origin, because of the time difference required by estimated spreading rates. It is assumed that the volcanic archipelago is built on normal MORB basement extruded at a diverging ridge during Aptian or early Albian time. The younger volcanism began after MORB basement had migrated off the ridge. The older volcanism ceased and the ocean floor subsided at about the time Hess Rise crossed the zone of high biological productivity near the mid-Cretaceous equator. Tectonic activity during the Late Cretaceous, mainly block-faulting, probably raised portions of the drowned archipelago above sea level, where subaerial erosion provided the clasts incorporated in the Cretaceous sequence at Site 466.

### ACKNOWLEDGMENTS

The authors thank Drs. Rodey Batiza, Bert E. Nordlie, and Robert Scott for reviewing this manuscript and making many helpful comments and suggestions.

### REFERENCES

- Andrews, A. J., 1977. Low temperature fluid alteration of oceanic layer 2 basalts, DSDP Leg 37. *Can. J. Earth Sci.*, 14:911.
- Baker, P. E., 1973. Islands of the South Atlantic. In Nairn, A. E. M., and Stehli, F. G. (Eds.), *The Ocean Basins and Margins*: New York (Plenum Press).
- Bass, M. N., 1976. Secondary minerals in oceanic basalt, with special reference to Leg 34, Deep Sea Drilling Project. In Yeats, R. S., Hart, S. R., et al., *Init. Repts. DSDP*, 34: Washington (U.S. Govt. Printing Office), 393-432.
- Bischoff, J. L., and Dickson, F. W., 1975. Seawater-basalt interaction at 200°C and 500 bars: implications for origin of sea-floor heavy-metal deposits and regulation of seawater chemistry. *Earth Planet. Sci. Lett.*, 25:385.
- Cann, J. R., 1971. Major element variations in ocean-floor basalts. *Phil. Trans. Royal Soc. London (ser. A)*, 268:495.
- Engel, A. E. J., Engel, C. G., and Haven, R. G., 1965. Chemical characteristics of oceanic basalt and the upper mantle. *Geol. Soc. Am. Bull.*, 76:719.
- Frey, F. A., Bryan, W. B., Thompson, G., et al., 1973. Petrological and geochemical results for basalts from DSDP Legs 2 and 3. *Trans. Am. Geophys. Union*, 54:1004.
- Hart, S. R., 1970. Chemical exchange between sea-water and deep ocean basalts. *Earth Planet. Sci. Lett.*, 9:269.
- , 1971. K, Rb, Cs, Sr and Ba contents and Sr isotope ratios of ocean floor basalts. *Phil. Trans. Royal Soc. London (ser. A)*, 268:573.
- Humphries, S. E., and Thompson, G., 1978. Hydrothermal alteration of oceanic basalts by seawater. *Geochim. Cosmochim. Acta*, 42:107.
- Jacobs, J. W., Korotev, R. L., Blanchard, D. P., et al., 1977. A well-tested procedure for instrumental neutron activation analysis of silicate rocks and minerals. *J. Radioanal. Chem.*, 40:93.
- Lancelot, Y., 1978. Relations entre evolution sedimentaire et tectonique de la plaque Pacifique de tuis le Cretace inferieur. *Mem. Soc. Geol. France*, 134.
- Lancelot, Y., and Larson, R. L., 1975. Sedimentary and tectonic evolution of the northwestern Pacific. In Larson, R. L., Moberly, R., et al., *Init. Repts. DSDP*, 32: Washington (U.S. Govt. Printing Office), 925-940.
- Ludden, J. N., and Thompson, G., 1978. An evaluation of the behavior of the rare earth elements during the weathering of sea-floor basalt. *Earth Planet. Sci. Lett.*, 43:85.
- Miyashiro, A., 1978. Nature of alkalic volcanic rock series. *Contr. Mineral. Petrol.*, 66:91.
- Mottl, M. J., and Holland, H. D., 1978. Chemical exchange during hydrothermal alteration of basalt by seawater. Experimental results for major and minor components of seawater. *Geochim. Cosmochim. Acta*, 42:1103.
- Scarfe, C. M., and Smith, D. G. W., 1977. Secondary minerals in some basaltic rocks from DSDP Leg 37. *Can. J. Earth Sci.*, 14:903.
- Scheidegger, K. F., and Stakes, D. S., 1977. Mineralogy, chemistry and crystallization sequence of clay minerals in altered tholeiitic basalts from the Peru Trench. *Earth Planet. Sci. Lett.*, 36:413.
- Slater, J. G., Anderson, R. N., and Bell, M. L., 1971. Elevation of ridges and evolution of the central eastern Pacific. *J. Geophys. Res.*, 76:7888.
- Seyfried, W. E., Jr., and Bischoff, J. L., 1979. Low temperature basalt alteration by seawater: an experimental study at 70°C and 150°C. *Geochim. Cosmochim. Acta*, 43:1937.
- Seyfried, W. E., Shanks, W. C., and Bischoff, J. L., 1976. Alteration and vein formation in Site 321 basalts. In Yeats, R. S., Hart, S. R., et al., *Init. Repts. DSDP*, 34: Washington (U.S. Govt. Printing Office), 385.
- Seyfried, W. E., Shanks, W. C., and Dibble, W. E., 1978. Clay mineral formation in DSDP Leg 34 basalt. *Earth Planet. Sci. Lett.*, 41:265.
- Shido, F., Miyashiro, A., and Ewing, M., 1971. Crystallization of abyssal tholeiites. *Contr. Mineral. Petrol.*, 31:251.
- Sun, S.-S., Nesbitt, R. W., and Sharaskin, A., 1979. Geochemical characteristics of mid-ocean ridge basalts. *Earth Planet. Sci. Lett.*, 44:119.